Surface segregation and ordering in III-V semiconductor alloys

Sverre Froyen and Alex Zunger
National Renewable Energy Laboratory, Golden, Colorado 80401
(Received 7 November 1995)

Using the first-principles total-energy pseudopotential method, we have studied the formation energy of the (001) $Ga_{1-x}In_xP$ alloy surface as a function of composition and reconstruction. The results are presented as $T=0$ surface stability diagrams that show the lowest energy reconstruction and cation occupation pattern as functions of the chemical potentials. Slightly different stability diagrams emanate depending on whether or not there is equilibrium between the surface and the bulk. The stability diagrams show a pronounced asymmetry between the Ga- and In-rich regions. The asymmetry is interpreted in terms of the size difference between In and Ga and the effect of this size difference on the bonding geometry. For surfaces in equilibrium with the bulk, we find a strong dependence of surface segregation on the surface reconstruction, and we predict a Ga enrichment of the surface in the moderate cation-rich limit and In enrichment in the anion-rich region. This result suggests a way to achieve abrupt interfaces in semiconductor heterostructures. For surfaces not in equilibrium with the bulk, we identify regions in the stability diagram where surface-induced CuPt ordering (both type *A* and type *B*) occurs.

I. INTRODUCTION

The structure of (001) III-V semiconductor surfaces is strongly dependent on the cation/anion ratio at the surface. For example, the (001) GaAs surface is observed to form a sequence of different reconstructions ranging from the $c(4\times4)$ and the (2×4) As-rich to the $(4\times2)/c(8\times2)$ and the (4×6) Ga-rich surfaces.[1,2] Each reconstruction can be understood as an attempt by the surface to accommodate its valence electrons either in Ga-As, As-As, or Ga-Ga bonding orbitals or in As dangling-bond orbitals. (001) surfaces of other III-V materials are less well studied but appear to show reconstructions similar to those of GaAs.[3,4] For semiconductor *alloy* surfaces, in addition to the cation/anion ratio, the concentration of the alloying elements must be considered. The combination of surface reconstruction and surface alloying leads to two new features absent from the surfaces of binary zinc-blende semiconductors: surface segregation and surface-induced atomic ordering.

By surface segregation of a given element, we mean enrichment of that element at a surface with respect to the bulk composition. Surface segregation has been extensively studied in metal alloys[5] where thermodynamic equilibrium is easily attained and where the impact of segregation at grain boundaries on metal strength was recognized early. Over the past 10 years, surface segregation studies have also been performed for semiconductor alloys,[6] and there has been recent interest because of an inability to achieve abrupt interfaces in artificially grown III-V superlattices and heterostructures. Sometimes, when growing heterostructures containing two materials *A* and *B*, one of the interfaces, say, the *A* on *B* interface, is abrupt whereas the *B* on *A* interface is diffuse. The nonabruptness of the *B* on *A* interface correlates with, and is assumed to be caused by, the surface segregation of material *A* during growth. This important technological problem has been studied for AlAs/GaAs and GaAs/InAs heterostructures, and empirical thermodynamic models have been fit to experiment (formulated using a single exchange energy or coefficient that models the energy change when a surface atom is swapped with a dissimilar bulk atom).[6–10]

Long-range cation or anion CuPt-type ordering has been observed in thick films for most pseudobinary III-V semiconductor alloys grown from vapor-phase constituents.[11] The ordering propagates deep into the film but has been shown to occur at the growth surface. It can be observed directly using electron or x-ray diffraction or indirectly through its effect on the band gap. CuPt-type ordering could, in principle, occur along any of the bulk-equivalent {111} directions. Experimentally, however, ordering along two of the directions, $[111]$ and $[\bar{1}\bar{1}\bar{1}]$, is observed much more often than that along the other two. The common type of ordering is labeled $CuPt_B$, and the other type is termed $CuPt_A$. We have previously studied the (001) $Ga_{0.5}In_{0.5}P$ alloy surfaces in the context of ordering.[12–15] We identified two possible thermodynamic sources for the observed $CuPt_B$ ordering. First, we identified a cation-terminated (2×2) surface reconstruction where the surface-layer cations would form a stable $CuPt_B$-like pattern. Second, we found that dimer-induced elastic deformation under anion-terminated (1×2) surfaces would cause the third subsurface layer cations to order in the $CuPt_B$ structure. The stability of these surfaces with respect to other types of surface reconstructions were not determined, however.

In this paper, we study atomic structure and $T=0$ formation energies of the $Ga_{1-x}In_xP$ (001) semiconductor alloy surface. $Ga_{0.5}In_{0.5}P$ alloys are usually grown on (lattice matched) GaAs substrates. We therefore constrain epitaxially our surfaces to GaAs, meaning that the surface lateral lattice parameters are those of GaAs. We consider the $c(4\times4)$, $\beta2(2\times4)$, $\beta2(4\times2)$, $\beta(4\times2)$, and (2×2) reconstructions. With the exception of the (2×2) reconstruction, these are well-studied, stable surface structures for the GaAs(001) surface and will be used to derive candidate alloy surface structures by replacing As with P and occupying the cation sites with various patterns of Ga and In. Other GaAs surface structures that have been observed[1,2] are either transitional, incom-

pletely understood, or have unit cells too large for our computational resources and will not be considered here. We also avoid the sometimes observed (2×1) and (1×2) reconstructions. Simple dimerized surfaces such as these do not satisfy the so-called electron counting rule[16] that characterizes low-energy surface structures. The electron counting rule simply states that under conditions of charge neutrality, the surface favors a semiconducting structure where all anion dangling bonds are filled and all cation dangling bonds are empty. We nevertheless include the (2×2) reconstruction, which is a modification of the (1×2) surface. This (2×2) recovers its semiconducting properties by making half of the cation dimers asymmetric.[12] For most of the reconstructions discussed above, we study the alloy formation in the top four atomic layers.

The resulting $T=0$ surface stability diagram is constructed from the $T=0$ formation energies versus chemical potentials. It provides detailed predictions of surface reconstruction patterns that are stable on the $Ga_{1-x}In_xP(001)$ alloy surface. Starting with the cation-rich surfaces, we find that the size difference between Ga and In leads to dramatic differences in the properties of the alloy surface relative to the GaAs(001) surface. The cation-terminated $\beta2(4\times2)$ reconstruction dominates the Ga-rich region of the alloy surface stability diagram. This reconstruction is also observed for Ga-rich GaAs surfaces. The $\beta2(4\times2)$ reconstruction is unstable, however, with respect to the anion-terminated $\beta2(2\times4)$ and cation-terminated (2×2) reconstructions in the In-rich region of the stability diagram. The $\beta2(2\times4)$ reconstruction dominates much of the more P-rich regions in the stability diagram, and we find a region of the double-layer, anion-terminated $c(4\times4)$ reconstruction to be stable in the extreme P-rich limit.

By comparing the surface composition to that of the bulk, we determine the type and magnitude of the alloy surface segregation. We observe a strong link between surface reconstruction and surface composition, producing Ga segregation for the $\beta2(4\times2)$ surface and In segregation for the $\beta2(2\times4)$ reconstruction. This link suggests that, by varying the P overpressure (and thereby the surface reconstruction) during the growth of semiconductor heterostructures, one can eliminate the negative effects of surface segregation on the interface abruptness.

In accord with our earlier studies,[12–15] we find strong $CuPt_B$-type ordering for the (2×2) and $\beta2(2\times4)$ reconstructions. The $\beta2(2\times4)$ results are new in that the previous study used a (2×1) cell. For the $c(4\times4)$ reconstruction, we find that $CuPt_A$-type ordering is strongly promoted for the cations in the second subsurface layer. The present study does not support the earlier prediction of $CuPt_A$ ordering in the second subsurface layer cations under the (2×2) surface.

II. METHOD OF CALCULATION

Constructing the $T=0$ surface stability diagram for $Ga_{1-x}In_xP$ is a matter of comparing the energy of the various possible reconstructions and cation occupation pattern and determining the one with the lowest energy. We use the first-principles pseudopotential method. Details, including plane-wave cutoffs, Brillouin zone sampling, etc., can be found in Ref. 13. For each reconstruction and occupation pattern, the energy is minimized with respect to atomic displacements. In order to compare energies of surfaces with different amounts of Ga, In, and P, we must specify the energy or the chemical potential of the Ga, In, or P atoms that must be removed or added when converting one surface into another. This assumes that the surface is in equilibrium with atomic reservoirs. For instance, an equation determining the coexistence line (by comparing the energies of the top four layers) of the cation-rich $\beta2(4\times2)$ GaP surface and the anion-rich $\beta2(2\times4)$ InP surface can be written as

$$E[\mathrm{GaP};\beta2(4\times2)]+\frac{14}{8}\,\mu_{\mathrm{In}}+\frac{6}{8}\,\mu_{\mathrm{P}}$$

$$=E[\mathrm{InP};\beta2(2\times4)]+\frac{12}{8}\,\mu_{\mathrm{Ga}}, \qquad (1)$$

where E is the calculated surface total energy per (1×1) surface unit cell and the coefficients of the chemical potentials (μ_{Ga}, μ_{In}, and μ_{P}) are determined by the number of atoms that are removed or added.[17] Similar equations can easily be generated for all pairs of structures. If the chemical potentials are free to vary without bounds, almost any surface reconstruction and composition can be stabilized. The chemical potentials must, however, obey certain restrictions. If the cation chemical potential is too high, cation precipitate can form. The (calculated) total energies of bulk Ga and In, therefore, place upper bounds on the cation chemical potentials. Similarly, the total energy of bulk P puts an upper bound on the P chemical potential. Furthermore, because a growing (dissolving) crystal adds (removes) bulk material and does not change the surface area, a crystal in steady state (i.e., not growing or dissolving) requires the chemical potentials to satisfy the equation

$$x\mu_{\mathrm{Ga}}+(1-x)\mu_{\mathrm{In}}+\mu_{\mathrm{P}}=E_{\mathrm{bulk}}(\mathrm{Ga}_{1-x}\mathrm{In}_x\mathrm{P};\alpha), \qquad (2)$$

where $E_{\mathrm{bulk}}(Ga_{1-x}In_xP;\,\alpha)$ is the bulk total energy (at composition x and structure α). Note that Eq. (2) contains the bulk energy even though growth only requires atomic exchange between the surface and the reservoirs. Normally, the bulk composition and structure are determined by $\mu_{\mathrm{Ga}}-\mu_{\mathrm{In}}$, but, because the above argument does not involve the surface structure, Eq. (2) is valid whether or not the bulk is in equilibrium. We will use the calculated total energies of bulk $Ga_{1-x}In_xP$ [taken as zinc blende GaP and InP constrained epitaxially to (001) GaAs and ordered $GaInP_2$ in the CuPt and chalcopyrite structures, as appropriate] to eliminate μ_{P}. We choose to measure μ_{Ga} and μ_{In} with respect to the total energies of bulk Ga and In, respectively. Because the bulk energies form upper bounds for the respective chemical potentials, they must both be negative although their difference can, of course, take any value.

Using experimental crystal structures[18] and optimizing the lattice parameters through energy minimization, we calculated formation energies of -0.92, -0.90, -1.34, and -1.22 eV for GaAs, InAs, GaP, and InP, respectively, somewhat higher than the experimental values, -0.85, -0.62, -1.04, and -0.64 eV.[19,20] Separate pseudopotential calculations, using more accurate, hard-core potentials and a 20-Ry plane-wave cutoff result in formation energies in good agreement with experiment for GaP and InP. This shows that the error is

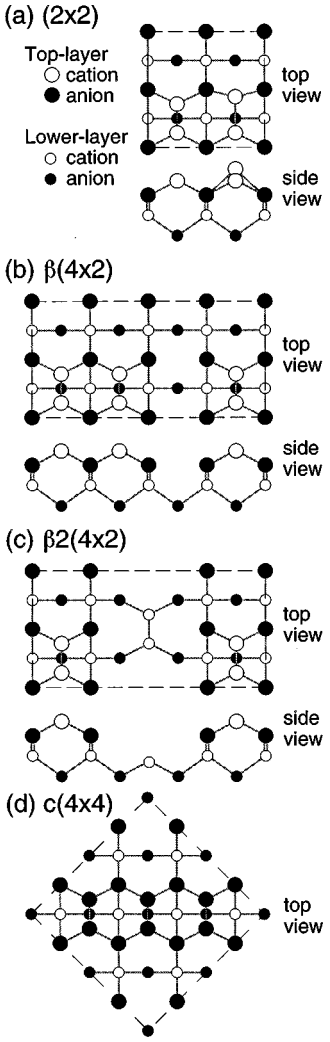

FIG. 1. Structural models for the (2×2), $\beta(4\times2)$, $\beta2(4\times2)$, and $c(4\times4)$ reconstruction for the GaAs(001) surface. Open (filled) circles denote cations (anions). The (2×4) reconstructions can be obtained from the (4×2) reconstructions by swapping cations and anions and rotating the surface 90°.

caused by the soft pseudopotentials and the relatively low plane-wave cutoff energy (10 Ry) used in the current study. Because the soft potentials give zinc-blende and zinc-blende-alloy energy differences in excellent agreement with the results from the hard-core potential calculations and also accurate linear augmented plane-wave calculations (see the discussion in Sec. III B), it seems likely that the formation energy errors are caused by underestimates of the binding energy of In-In and P-P bonds. The overestimate of the formation energies is of concern because it determines the chemical potential bounds. If we assume that the error only affects the energy of the elements, we can correct by lowering the energy of In and P by 0.3 eV each. The chemical potential boundaries of In and P would shift by the same amount, reducing the accessible range by 0.3 eV for GaP and 0.6 eV for InP. Note, however, that the error may affect the dimer binding energies as well. The current results should therefore be taken as representative of nonlattice-matched III-V semiconductor alloys and not as a completely accurate description of $Ga_{1-x}In_xP$. Note also that for finite T, the chemical potential limits are determined by the free rather than the internal energy, further reducing the accessible range.

III. INDIVIDUAL STABILITY DIAGRAMS

In order to better understand the resulting stability diagram, it is useful to consider some special cases that allow us to examine $T=0$ surface energies as functions of single variables, i.e., μ_{Ga}, μ_{In}, and $\Delta\mu=\mu_{Ga}-\mu_{In}$. We first consider the surfaces of the binary constituents, GaP and InP. Next, we consider the alloy, but for one reconstruction at a time. As we shall see, the individual surface reconstruction is the determining factor in how sites are occupied, which in turn determines surface segregation and ordering. Discussing one reconstruction at a time is, therefore, natural. In Sec. IV, we will combine the results into a global stability diagram.

A. (001) surfaces of GaAs, GaP/GaAs, and InP/GaAs

Because we are ultimately interested in the alloy, which is grown on GaAs, we constrain the lateral lattice parameters of GaP and InP to match those of GaAs. GaP is therefore laterally expanded and InP is laterally compressed. The lattice parameter perpendicular to the surface is determined by energy minimization. Schematic models of the various reconstructions are shown in Fig. 1, and their relative surface formation energies are plotted as functions of the cation chemical potential in Fig. 2. Figure 2 also includes results for GaAs from Refs. 21 and 22. For each material, we have indicated the allowed range of the chemical potential as obtained using the calculated total energies of the condensed phases of Ga, In, P, and As.[23] For all three surfaces, the cation-terminated, three-dimer plus missing dimer $\beta(4\times2)$ reconstruction has a higher energy than the two-dimer plus subsurface dimer $\beta2(4\times2)$ reconstruction. For GaAs, the $\beta2(4\times2)$ surface is stable over a narrow 0.15-eV chemical potential range in the Ga-rich limit. For the laterally expanded GaP surface, the stability range of the $\beta2(4\times2)$ phase is significantly enlarged, whereas for the compressed InP surface, this reconstruction is unstable with respect to a monolayer cation terminated (2×2) reconstruction and a P-terminated, two-dimer plus subsurface dimer $\beta2(2\times4)$ reconstruction. These differences can be understood in terms of cation-dimer relaxation, as described below. For all three materials, we find that the $\beta2(2\times4)$ reconstruction is stable as the surfaces become more anion rich, and that the P-terminated three dimers plus missing dimer on P $c(4\times4)$ reconstruction is stable in the extreme P-rich limit.

B. Bulk stability diagram

The *bulk* $T=0$ relative formation energies for epitaxially strained GaP, InP, and $GaInP_2$ are shown in Fig. 3. As the chemical potential difference $\mu_{Ga}-\mu_{In}$ changes from In rich to Ga rich, the equilibrium bulk structure changes from InP, to chalcopyrite $GaInP_2$, and then to GaP. The transition points are $\Delta\mu=\mu_{Ga}-\mu_{In}=-0.15$ and -0.03 eV, respectively. The experimentally observed CuPt-ordered $GaInP_2$ is 25.5 meV per atom higher in energy than the chalcopyrite structure with the same composition and is therefore unstable in bulk form for any value of the chemical potentials. Our

value for the CuPt-chalcopyrite energy difference is in good agreement with the value 28.6 meV per atom from a recent calculation by Lu *et al.*[24] and the chalcopyrite formation energies, 7.8 and −15.0 meV per atom with respect to incoherent and epitaxially coherent (on GaAs) binaries, respectively, are also in good agreement with previous calculations, 7.5 meV per atom[24] and −15.7 meV per atom.[25] The value $\Delta\mu_b=-0.09$ eV is the point where the bulk composition crosses over from In rich to Ga rich. This point will serve as a reference for assessing surface segregation, below.

C. The (2×2) alloy surface

Next, consider the monolayer cation coverage (2×2) surface reconstruction (Fig. 4). As shown in Fig. 2, this reconstruction may be stable for laterally compressed InP but unstable for expanded GaP. The (2×2) unit cell contains a symmetric, low cation dimer with its atoms in planar sp^2 bonding configurations [with sites labeled l_1 and l_2 in Fig. 4(b)], and an asymmetric raised dimer with one cation in a medium-low (m) sp^2 configuration and the other in a high (h) pyramidal s^2p^3 configuration. We have previously[12] calculated the energy for $Ga_{1-x}In_xP$ (2×2) surfaces containing zero, two, and four In atoms in the four-atom 2×2 unit cell (the remainder being Ga). For surfaces containing two In atoms, we found that a pattern with Ga occupying the l_1 and l_2 sites and In occupying the m and h sites had the lowest energy. This occupation pattern corresponds to bulk $CuPt_B$ ordering. We now expand our earlier calculation to include (2×2) surfaces containing one and three surface In atoms per cell. We also allow for In in the second subsurface layer in addition to Ga [on the sites labeled A and B in Fig. 4(b)]. As before, GaAs is used as substrate below the top three atomic layers. For the new surfaces, the minority surface atom can occupy one of the four inequivalent sites in the 2×2 cell (l_1, l_2, m, or h). Based on a spin model[14] fit to our previous results, we expect that an In atom would prefer the medium-low site on the raised dimer (m), and a Ga atom would prefer one of the sites on the low dimer (l_1 or l_2). For Ga on the A and B sites, the model fits the present pseudopotential results within 3 meV per surface atom. An outstanding feature of the spin model is strongly dominant on-site interaction terms and almost negligible pair interactions. As we shall see below, this is common to all the surface reconstructions and, to the extent that pair interactions can be completely ignored, causes all ordered surface alloys to have primitive cells equal to that of the associated surface reconstruction.

Figure 4(a) summarizes our results. It shows the calculated relative surface energies for the (2×2) surfaces as a function of the chemical potential difference $\Delta\mu=\mu_{Ga}-\mu_{In}$. Each line in the figure is labeled according to the sites occupied by Ga. For instance, *lhm* means that the sites l_1, l_2, h, and m are occupied by Ga and the sites A and B are occupied by In. The lowest-energy surface structures can be grouped into separate regions with transition points indicated by the vertical arrows in Fig. 4(a). Below $\Delta\mu=-0.22$ eV, all the surface and subsurface sites are occupied by In. At −0.22 eV, both cations on the low dimer sites change from In to Ga. Between −0.22 eV and −0.07 eV, the low-energy structure

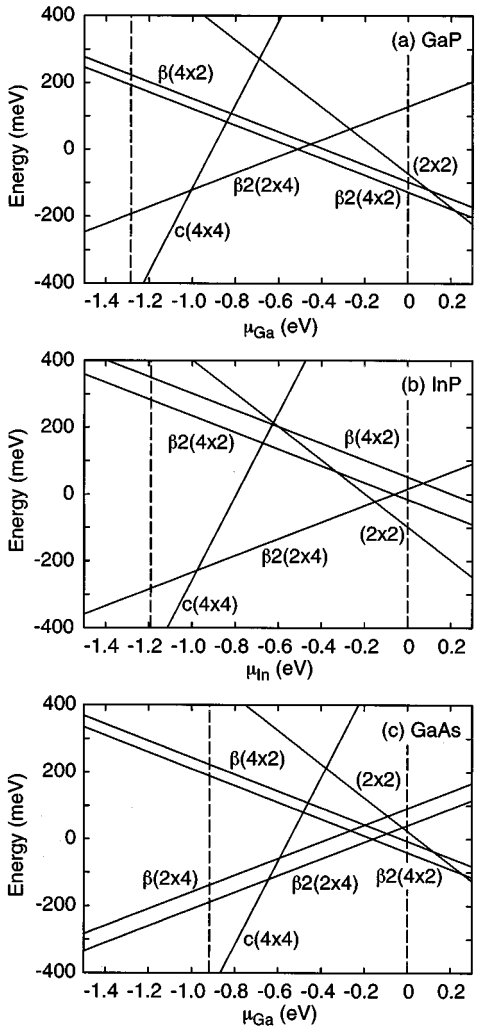

FIG. 2. Relative formation energy per 1×1 unit cell for (a) GaP on GaAs, (b) InP on GaAs, and (c) GaAs(001) surfaces as a function of the cation chemical potential (with respect to solid Ga and In). The dashed vertical lines indicate the limits of the thermodynamically allowed range. The reference composition corresponds to a surface with equal amounts of cations and anions and the zero of energy is chosen for presentation purposes.

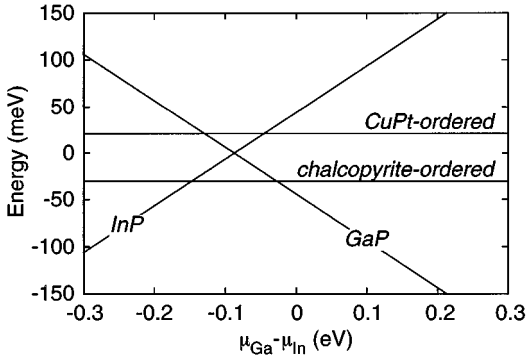

FIG. 3. Relative formation energy per two atoms for bulk GaP, InP, and ordered chalcopyrite-like and CuPt-like $GaInP_2$ as a function of the Ga/In chemical potential difference. The reference composition and the zero of energy are chosen for presentation purposes.

is a $CuPt_B$-ordered $Ga_{0.5}In_{0.5}P$ surface layer with In in the second subsurface layer. At -0.07 and -0.05 eV, the sites in the subsurface layer change their occupation while the surface layer remains $CuPt_B$ ordered. Finally, at 0.18 and 0.20 eV, the cations on the raised dimer sites change from In to Ga and the surface changes from $CuPt_B$ to pure GaP. In our earlier study using a valence force field model,[13,14] we found an energy difference of 103 meV per surface atom between the two subsurface $CuPt_A$ variants: Ga on A sites and In on B sites for the low-energy variant and and the opposite for the high-energy variant. Combined with the spin model results, this suggested that the layer might be strongly $CuPt_A$ ordered.[14] Here, the energy difference is only 22 meV per surface atom. The ordering in the subsurface layer is therefore much reduced and is negligible at typical growth temperatures. At the reference value $\Delta\mu_b=-0.09$ eV, where the bulk composition is 1/2, the surface layer composition is 1/2 with Ga on l_1 and l_2 and In on h and m. The subsurface layer is pure In at $T=0$, but the proximity of $\Delta\mu_b$ to both the A and B transitions will make the sublayer only slightly In rich at finite T.

D. The $\beta 2(4\times2)$ alloy surface

Reducing the cation content, we next study the $\frac{3}{4}$-monolayer cation-terminated $\beta 2(4\times2)$ structure (Fig. 5).

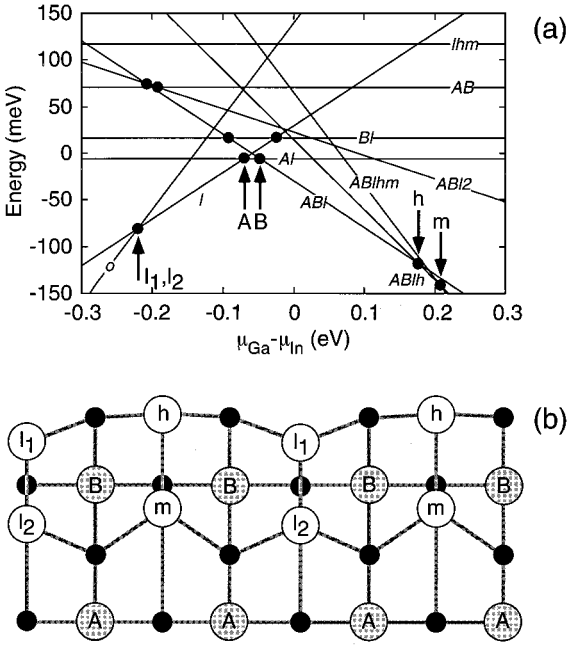

FIG. 4. Relative formation energy per 1×1 unit cell as a function of the $\mu_{Ga}-\mu_{In}$ chemical potential difference (a) and top view of the structure of the uppermost four layers (b) for $Ga_{1-x}In_xP(001)$ surfaces in the (2×2) reconstruction. Each line in part (a) is labeled according to which sites [with reference to part (b)] are occupied by Ga. Each arrow and small solid circle indicates the chemical potential value at which a particular site (as labeled) changes its occupation from In to Ga (from left to right). The reference composition corresponds to a surface with equal amounts of Ga and In, and the zero of energy is chosen for presentation purposes. In part (b), the solid black circles show the position of P atoms, the open circles represent top-layer cations, and the shaded circles indicate second-layer cations.

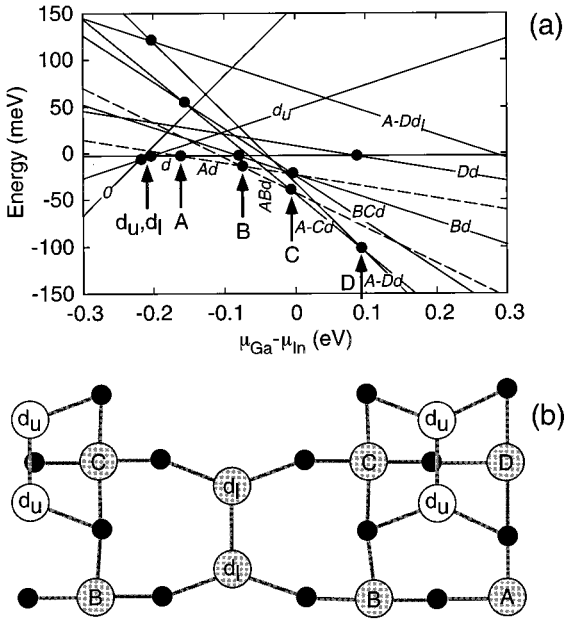

FIG. 5. Relative formation energy per 1×1 unit cell (a) and top view of the structure of the uppermost four layers (b) for the $\beta 2(4\times2)$ reconstruction. Dashed lines correspond to structures whose energy has been calculated using an Ising model. See also the caption for Fig. 4.

This reconstruction contains three cation dimers per unit cell, two in the surface layer, labeled d_u (for upper) in Fig. 5(b), and one in the second subsurface layer, labeled d_l. Both the surface dimers and the subsurface dimer sites change their occupation around $\Delta\mu=\mu_{Ga}-\mu_{In}=-0.21$ eV.[26] Given that it should be easier to accommodate the larger In atoms at the surface than in the bulk, it is perhaps surprising that the surface dimer sites change from In to Ga at a more negative value of $\Delta\mu$ than do either the subsurface atoms (with their fourfold coordination), bulk, or, on the average, the dimers on the more densely packed (2×2) surface. The highly negative $\Delta\mu$ value for the dimer transformation point can be understood, however, by noting that Ga is better able to achieve planar sp^2 bonding geometries between the underlying P atoms than is the larger In atom. The electronic configuration of the dimers on the $\beta 2(4\times2)$ surface is the same as that of the low dimer on the (2×2) surface, and this fact is reflected in their very similar transition values [compare the l_1,l_2 transition in Fig. 4(a) with the d_u,d_l transition in Fig. 5(a)].[27] The $\beta 2(4\times2)$ surface contains only low dimers, whereas, on the (2×2) surface, half the In can remain relatively unconfined on the electron-rich $sp^2-s^2p^3$ high dimer. This gives the (2×2) surface an energy advantage when the In content is high and helps explain why the $\beta 2(4\times2)$ surface is stable for GaP but unstable for InP.[28] One can also observe, in Fig. 5(b), how the cation dimers push the P atoms outwards. The dimer-induced elastic relaxation makes the subsurface sites inequivalent in terms of size and causes the subsurface sites $(A-D)$ to transform over a range of chemical potential between -0.16 and 0.10 eV. The sites directly underneath the dimers (C and D) have more space than the sites between the dimer rows (A and B), as reflected in the sequence at which the sites transform.

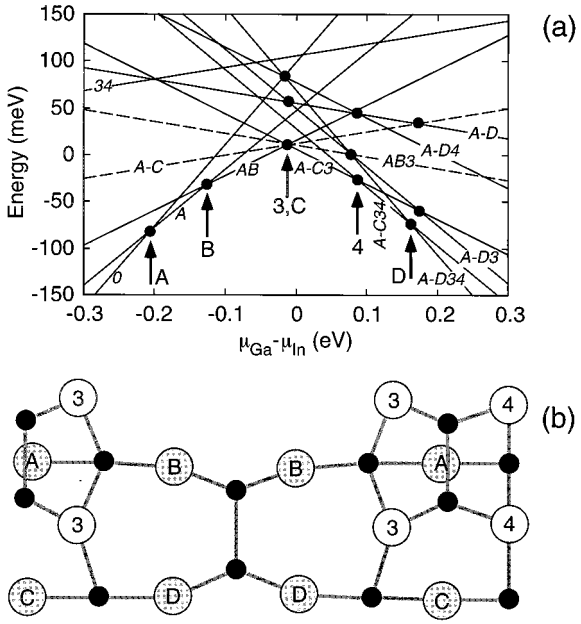

FIG. 6. Relative formation energy per 1×1 unit cell (a) and top view of the structure of the uppermost four layers (b) for the $\beta 2(2\times4)$ reconstruction. Dashed lines correspond to structures whose energy has been estimated using an Ising model. See also the caption for Fig. 4.

In the chemical potential range between transitions *B* and *C*, the occupation of the subsurface sites *A*, *B*, *C*, and *D* corresponds to $CuPt_A$ ordering, but, because the d_l sites contain Ga, the subsurface layer composition is not $\frac{1}{2}$. In a later section, we will discuss ordering at finite temperatures, and there we will see that forcing the layer composition to be $\frac{1}{2}$ will fix the $\Delta\mu$ at the *B* transition, leading to small values for the $CuPt_A$ *as well as* the $CuPt_B$ ordering parameter. Note that using a layer (In) composition of $\frac{3}{8}$ will produce a much larger $CuPt_A$ ordering parameter. Note also that elastic relaxations induced by the d_l dimer may promote $CuPt_A$ ordering below the second subsurface layer as well.

We note again that the $\Delta\mu$ value at which a given site changes its occupation is approximately independent of the occupation at the other sites. This can be observed from Fig. 5(a) by noting that the small solid circles, each denoting the occupation change of a single site, are stacked approximately vertically.[29]

At the bulk reference point $\Delta\mu_b=-0.09$ eV, the surface dimers d_u are all Ga. The subsurface dimers D_l and the *A* site are also Ga while the *B*, *C*, and *D* sites contain In. Simple counting leads to an overall (In) composition of $\frac{5}{12}$ for the two layers. At finite *T*, the In concentration will be even smaller because of the proximity of $\Delta\mu_b$ to the *B* transition. The $\beta 2(4\times2)$ surface therefore segregates Ga.

E. The $\beta 2(2\times4)$ alloy surface

Removing additional surface cations, we obtain the $\frac{3}{4}$-monolayer, anion-terminated $\beta 2(2\times4)$ surface (Fig. 6). The $\beta 2(2\times4)$ surface is identical to the $\beta 2(4\times2)$ surface, but with cations and anions swapped [compare Fig. 6(b) and Fig. 5(b)]. The surface is terminated by P dimers and the first subsurface layer contains four threefold [labeled "3" in Fig. 6(b)] and two fourfold (labeled "4") coordinated cations per unit cell.[30] The cations in the third subsurface layer are labeled *A*–*D*, and are all fourfold coordinated. Relative surface formation energies are given in Fig. 6(a). Considering first the top cation layer sites (the first subsurface layer), the threefold-coordinated cations change their occupation at $\Delta\mu=\mu_{Ga}-\mu_{In}=-0.01$ eV and the fourfold-coordinated cations in the top cation layer transform at 0.09 eV. Each dimerized P atom has five electrons and therefore prefers s^2p^3 bonding configurations with 90° bond angles. Because such bond angles are more easily achieved with the longer In-P bond lengths, In occupation is favored on site "4." Another manifestation of the bonding configuration can be observed in Fig. 6(b), where the P dimers pull the underlying cations inwards. Although the next cation layer (third subsurface layer) have bulklike environments, dimer-induced elastic relaxations again cause the sites to be inequivalent. They transform over a range of $\Delta\mu$ as indicated by the arrows in Fig. 6(a). Note that now the cations *underneath* the dimers (sites *A* and *B*) transform at the more negative $\Delta\mu$. The transformation range for the $\beta 2(4\times2)$ is also larger than that for the $\beta 2(4\times2)$ surface.

Between $\Delta\mu=-0.13$ eV (where the *B* site transforms) and -0.01 eV (where the *C* site changes occupation), the subsurface cation pattern is $CuPt_B$-like, with Ga on the *A* and *B* sites and In on the *C* and *D* sites. The more complex reconstruction, therefore, leads to qualitatively the same result as our earlier study,[12–15] where we used a simpler (1×2) reconstruction.

At the reference point $\Delta\mu_b$ where the bulk composition is $\frac{1}{2}$, the first subsurface layer cation sites "3" and "4," as well as the third subsurface layer cation sites *C* and *D*, are all occupied by In with only the sites *A* and *B* occupied by Ga. The composition in the top four layers is therefore $\frac{8}{12}$, which shows that the $\beta 2(2\times4)$ surface segregates In.

F. The $c(4\times4)$ alloy surface

The $c(4\times4)$ reconstructed surface is terminated by 1 and $\frac{3}{4}$ monolayers of P. The surface layer is dimerized with every fourth dimer missing. It reconstructs in the $c(4\times4)$ instead of the $\beta(4\times2)$ pattern to lower its electrostatic energy.[22] Because the topmost cation layer for this surface is already the second subsurface layer, we have restricted our investigation to the alloying of this single layer. As shown in Fig. 7(b), the layer contains three inequivalent sites, labeled *A*, *B*, and *C*. All three sites are fourfold coordinated. The energetics of the layer, shown in Fig. 7(a), are determined by dimer-induced elastic relaxations similar to those for the $\beta 2(2\times4)$ surface. The smaller space on sites underneath the dimers, *A* and *B*, favors the occupation of Ga atoms. The *A* sites are underneath two dimers while the *B* sites neighbor a missing dimer, causing the *A* site to transform at $\Delta\mu=\mu_{Ga}-\mu_{In}=-0.44$ eV, compared to -0.05 eV for the *B* site. The *C* site transforms at 0.20 eV, giving a transformation range of 0.64 eV. This range is much larger than that of the third sublayer underneath the $\beta 2(2\times4)$ surface, presumably caused by the stronger effect of three aligned dimers.

In the range $-0.05<\Delta\mu<0.20$ eV, the *A* and *B* sites are occupied by Ga and the *C* sites by In. This pattern corresponds to $CuPt_A$ ordering.

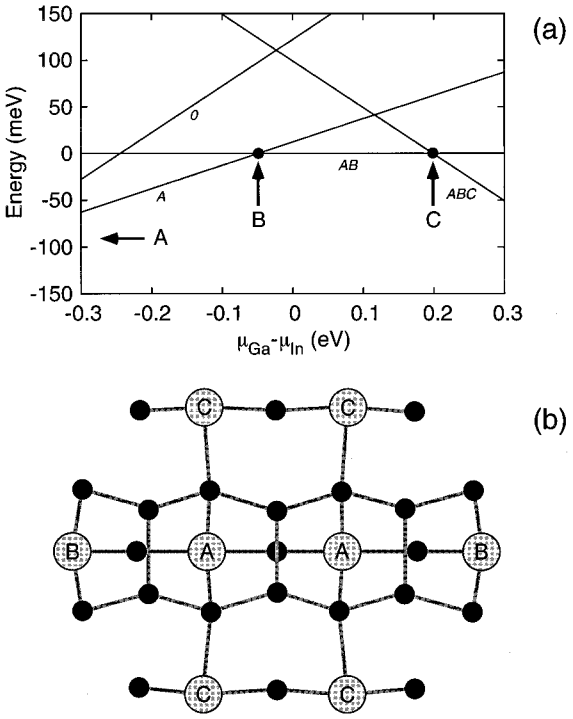

FIG. 7. Relative formation energy per 1×1 unit cell (a) and top view of the structure of the uppermost four layers (b) for the $c(4\times4)$ reconstruction. See also the caption for Fig. 4.

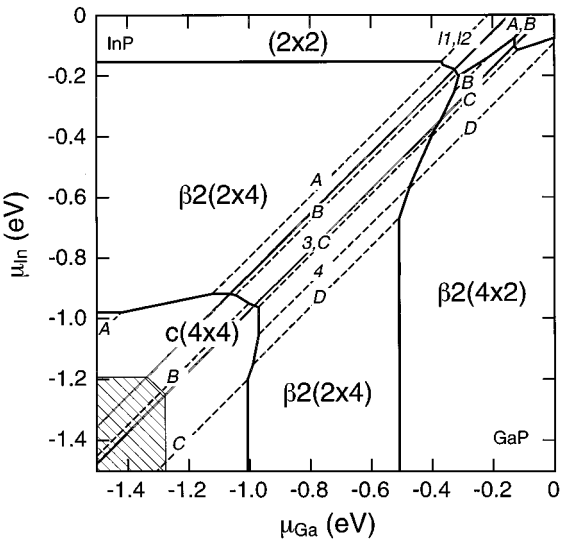

FIG. 8. $T=0$ surface stability diagram as a function of the Ga and In chemical potentials for the uppermost four layers of the $Ga_{1-x}In_xP(001)$ surface. The surface layers are assumed to be in equilibrium with the bulk. The solid black lines separate regions of different reconstructions (as labeled), and the dashed lines indicate composition changes within a given reconstruction. The latter lines are labeled according to Figs. 3–5. The solid gray lines show the bulk composition changes (see Fig. 3), and the cross-hatched region is thermodynamically inaccessible because μ_P exceeds the energy of bulk phosphorus.

At the reference value $\Delta\mu_b=0.09$ eV, where the bulk composition is $\frac{1}{2}$, only the A sites are occupied by Ga. This gives a layer (In) composition of 6/8. The $c(4\times4)$ surface, therefore, segregates In, although the proximity of the B transition will strongly reduce the segregation at finite temperature.

IV. THE GLOBAL (001) SURFACE STABILITY DIAGRAM

We next combine the results of Figs. 2–7. Because this involves comparing surfaces with different numbers of cations, the Ga and In concentrations are now independent, and a line in a previous figure converts to a surface in the two-dimensional space of $\mu_{Ga}-\mu_{In}$ and $\mu_{Ga}+\mu_{In}$ or, equivalently, μ_{Ga} and μ_{In}. For each pair of chemical potential values, the stable surface configuration is determined by selecting the one with the lowest energy.

A. Surface reconstruction and surface segregation at $T=0$

As discussed previously, for a surface in complete equilibrium with its bulk, μ_P is determined as a function of μ_{Ga} and μ_{In} by the bulk structure with the lowest energy (according to Fig. 3). The result (Fig. 8) is a prediction of the structure and composition (including the occupation pattern) of uppermost four surface layers. (Deeper layers are considered to behave energetically like bulk.) The heavy solid lines in the figure indicate boundaries between different reconstructions. A change in composition without an attendant reconstruction change is indicated by the dashed lines and is labeled according to Figs. 4–7. As expected from our discussion of the binary surfaces (Fig. 2), the cation-terminated (2×2) surface is unstable under Ga-rich conditions with respect to the $\beta2(4\times2)$ surface. However, under more In-rich conditions, the (2×2) CuPt-ordered $GaInP_2$ surface and the InP surface may be stable. Conversely, the cation-terminated $\beta2(4\times2)$ surface is stable only in the Ga-rich region. For more negative values of the cation chemical potentials, the P-terminated $\beta2(2\times4)$ surfaces become stable. In general, pure GaP is found in the lower right-hand corner of Fig. 8, pure InP in the upper left-hand corner, and mixed compositions in between. Comparing the composition of the surface to that of the bulk, the (2×2) surface layer tends to have the bulk composition, the $\beta2(4\times2)$ surface layer is Ga rich, and the $\beta2(2\times4)$ first subsurface layer is In rich. The cation layers below the first subsurface layer are all bulklike in their composition. As argued in the discussion of the energetics of each reconstruction, it is likely that the strong asymmetry between In and Ga is caused by the relative difficulty or ease by which the In/Ga atoms can occupy the low dimers on the cation-terminated surfaces. Thus, we expect that the surface stability diagram in Fig. 8 is typical of III-V common-anion lattice-mismatched alloys.

B. Surface segregation at finite T

We have noted several times that the occupation of a particular site is largely determined by the properties of the site itself and is independent of the occupation of other sites. Furthermore, the energy gained or lost by changing the occupation of a particular site i is simply the difference between the current value of $\Delta\mu=\mu_{Ga}-\mu_{In}$ and the value $\Delta\mu_i$ at which the site would change its occupation at $T=0$ (see Figs. 4–7). The finite temperature occupation of a site i is, therefore, $e^{\pm(\Delta\mu-\Delta\mu_i)/kT}/(1+e^{\pm(\Delta\mu-\Delta\mu_i)/kT})$. For growth on

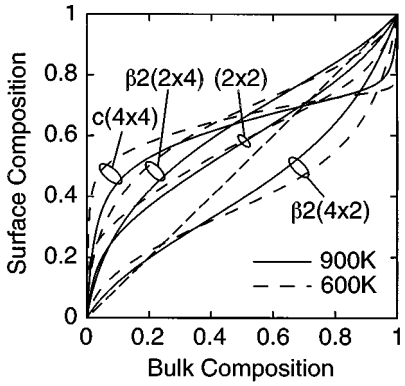

FIG. 9. Surface composition as a function of bulk composition for the $Ga_{1-x}In_xP(001)$ surface in the indicated reconstructions at $T=600$ and 900 K. The surface composition is that of the uppermost four layers.

the $\beta 2(2\times4)$ surface, and assuming that the growth takes place roughly in the middle of the $GaInP_2$ bulk region (i.e., at $\Delta\mu=-0.1$ eV), the energy term $\Delta\mu-\Delta\mu_i$ for site "3" (see Fig. 6) is -0.1 eV and for site "4" is -0.2 eV. These values are in rough agreement with the values -0.15 to -0.22 eV inferred from the thermodynamic modeling of observed surface segregation at (001) $Ga_xIn_{1-x}As$ surfaces.[6,9,10] Nagle *et al.*[9] noted that their data for growth on cation-terminated (4×2) surfaces seemed to indicate a reduced segregation of In, also in accord with our calculation.

We can use the above model to produce quantitative results for segregation at finite temperatures. A comparison of the composition in the top two surface layers with that of the bulk is shown in Fig. 9 for two temperatures, 600 and 900 K. The relationship between the bulk chemical potential and composition was determined using the regular solution model.[31] The energy of the epitaxially constrained random alloy was determined using a linear combination of the bulk structures shown in Fig. 3 with coefficients determined by the tetrahedral cluster probabilities of the random alloy ($\frac{1}{16}$, $\frac{3}{8}$, $\frac{1}{2}$, and $\frac{1}{16}$ for GaP, chalcopyrite, CuPt, and InP, respectively).[32] The surface composition is that of the four surface layers shown in Figs. 4–7. Figure 9 confirms our earlier discussions and shows that, in general, the $c(4\times4)$ and $\beta 2(2\times4)$ segregate In, the $\beta 2(4\times2)$ segregates Ga, while the (2×2) reconstruction is relatively nonsegregating. Not shown in the figure but evident in our calculations is that the surface layer is much more strongly segregating than the subsurface layer. Notice how all the curves in Fig. 9 have derivatives of less than one for intermediate compositions. The composition of the surface, therefore, changes more slowly than that of the bulk. This surface composition pinning is caused by the fact that the chemical potential range over which the surface transforms its composition from In to Ga is much larger than that of the bulk (compare Figs. 4–7 to Fig. 3).

Finally, our results suggest a way to create abrupt interfaces in semiconductor heterostructures. If the observed nonabruptness in, e.g., GaAs on InAs growth is caused by interfacial mixing due to In surface segregation, it can perhaps be overcome by changing the chemical potential of both the anion and the cations during growth. The In-rich layers could be grown on the $\beta 2(2\times4)$ surface, where In would segregate to the surface, and the Ga-rich layers could be grown on the $\beta 2(4\times2)$ surface, where Ga should segregate. The surface segregation effect should then work to make both the In on Ga and the Ga on In interfaces abrupt. Tournie, Trampert, and Ploog[33] have demonstrated that growth on $\beta 2(4\times2)$ surfaces is possible, although they were using the reduced anion diffusion rate of the cation-terminated $\beta 2(4\times2)$ to increase the critical thickness of strained InAs layers.

C. Surface ordering at $T=0$

Figures 4–7 show that two-dimensional CuPt ordering is possible in the near-surface layers. Figure 3 shows, on the other hand, that chalcopyrite-ordered bulk $GaInP_2$ has a lower energy than that of CuPt-ordered bulk. In order for a surface ordering mechanism to lead to three-dimensional CuPt ordering in thick films, there can, therefore, be no diffusion in the interior of the sample. Such diffusion would destroy the CuPt ordering and lead to chalcopyrite ordering (at very low T) or a random alloy (at higher T). Equilibrium between the bulk and the surface can, therefore, not be present if CuPt ordering is observed. This lack of equilibrium modifies the surface stability diagram. Consider growth where diffusion rates restrict equilibrium to only the top n cation layers. As before, the P chemical potential μ_P is determined according to Eq. (2) by the bulk composition and structure. The surface structure and composition must, however, remain consistent with the bulk. To see this, imagine changing μ_P slightly so that the crystal grows (or shrinks). The nth layer (before the growth), which previously was part of the equilibrium, is now out of equilibrium with the surface. Such a situation clearly only makes sense if the nth layer, i.e., the deepest layer in equilibrium with the surface, has the composition and structure of the bulk. In the calculation of the stability diagram, we must therefore only include structures whose occupation patterns in layer n and below are like bulk. Motivated by experiment, we consider the bulk structures GaP, InP, and CuPt-ordered $GaInP_2$. For each of these bulk structures, a surface stability diagram is computed, and the stability region of the surface whose nth cation layer composition and structure is consistent with (same as) the bulk is extracted and shown in Fig. 10 for $n=1$ and Fig. 11 for $n=2$ [$n=1$ for the $c(4\times4)$ surface]. Thus, Figs. 10 and 11 represent stability diagrams for surfaces where diffusion is limited to the top two and the top four monolayers, respectively. The gross features of the resulting stability diagram resembles Fig. 8 with some minor shifts of boundaries. Some regions overlap slightly, indicating hysteresis, and gaps are seen where no surface structure consistent with the three bulk structures was found. Regions of CuPt-ordered $GaInP_2$ exist in Fig. 10 for the (2×2) reconstruction and in Fig. 11 for the $\beta 2(2\times4)$ and the $c(4\times4)$ surfaces, with the latter being A type. For the $\beta 2(4\times2)$ surface, as discussed in Section III D, perfect CuPt ordering does not exist.

D. Surface ordering at finite T

We can use the thermodynamic model discussed in Section IV B, above, to calculate the occupation or composition of each site as a function of temperature. For each surface reconstruction, we focus on the layer that shows the strongest tendency to order. This includes the surface layer for the

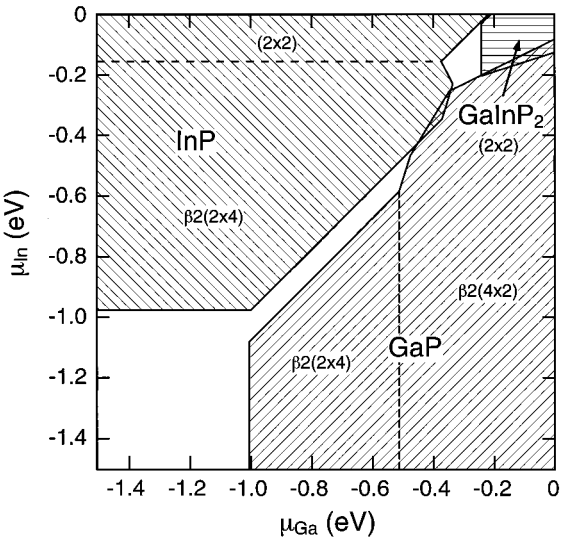

FIG. 10. $T=0$ surface stability diagram of the $Ga_{1-x}In_xP(001)$ surface as a function of the Ga and In chemical potentials for surfaces where diffusion is limited to the uppermost two monolayers. The figure is a composite of three separate calculations and shows the stability region of GaP, InP, and CuPt-ordered $GaInP_2$ when the surface layer is *not* in equilibrium with the bulk.

(2×2) surface, the second subsurface layer for the $\beta2(4\times2)$ and the $c(4\times4)$ surfaces, and the third subsurface layer for the $\beta2(2\times4)$ surface. The chemical potential $\Delta\mu=\mu_{Ga}-\mu_{In}$ is calculated as a function of T by requiring that the average composition is $\frac{1}{2}$. $CuPt_B$ and $CuPt_A$ order parameters are calculated from the appropriate site composition differences. The results are shown in Fig. 12. The surfaces with the strongest tendency for ordering are the $CuPt_B$-ordered (2×2) surface [Fig. 12(a)] and the $CuPt_A$-ordered $c(4\times4)$ surface [Fig. 12(d)]. The current (2×2) results are identical to our previous results shown in Fig. 6(b) in Ref. 14. As discussed in Sec. III D, our choice of layer composition causes the $\beta2(4\times2)$ surface [Fig. 12(b)] to order weakly in the second subsurface layer with nonzero order parameters for both $CuPt_A$ and $CuPt_B$ ordering. The $\beta2(2\times4)$ surface [Fig. 12(c)] is relatively strongly $CuPt_B$ ordered. The $\beta2(2\times4)$ surface has only half the number of ordering-inducing top-layer dimers as that of the surface used in our earlier calculation [see Fig. 8(b) in Ref. 14], where a much larger degree of order was observed. Obviously, low diffusion rates combined

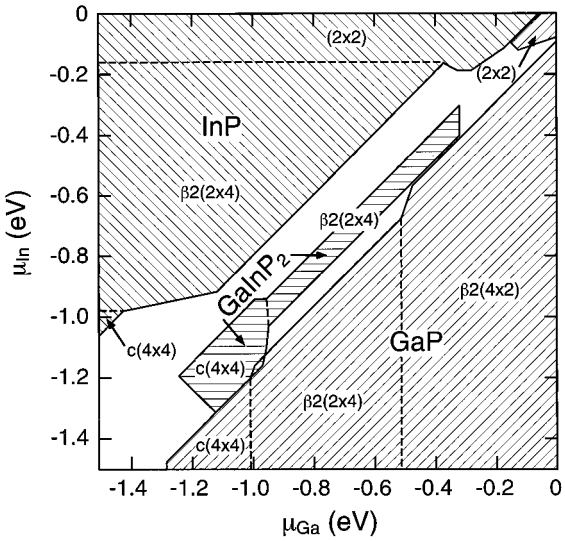

FIG. 11. $T=0$ surface stability diagram of the $Ga_{1-x}In_xP(001)$ surface as a function of the Ga and In chemical potentials for surfaces where diffusion is limited to the uppermost four monolayers. The figure is a composite of three separate calculations and shows the stability region of GaP, InP, and CuPt-ordered $GaInP_2$ when the surface layer is *not* in equilibrium with the bulk.

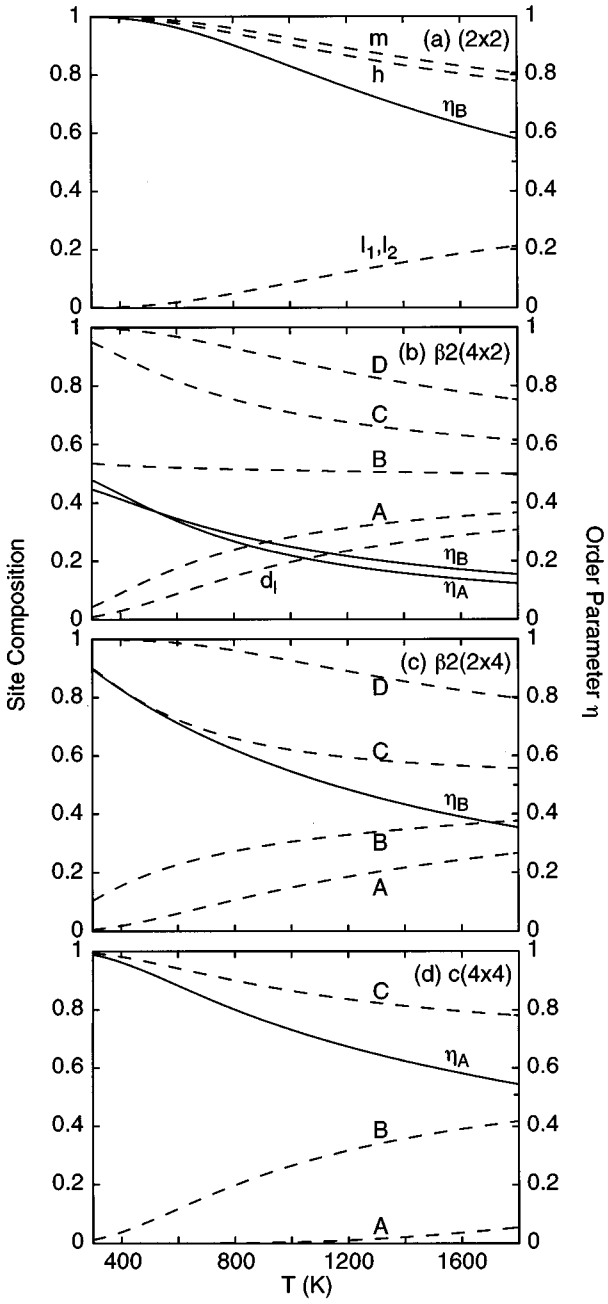

FIG. 12. Site compositions and CuPt ordering parameters as a function of temperature for (a) the surface layer for the (2×2) reconstruction, (b) the second subsurface layer for the $\beta2(4\times2)$ reconstruction, (c) the third subsurface layer for the $\beta2(2\times4)$ reconstruction, and (d) the second subsurface layer for the $c(4\times4)$ reconstruction of the $Ga_{1-x}In_xP(001)$ surface.

with high growth rates will reduce the degree of order that is achieved in the subsurface layers. The observed degree of order for the $c(4\times4)$ and $\beta2(2\times4)$ surfaces may therefore be much less than predicted in Figs. 12(c) and 12(d).

V. SUMMARY

We have performed total-energy calculations for (001) $Ga_{1-x}In_xP$ surfaces in the cation-terminated (2×2) and $\beta2(4\times2)$ reconstructions and the anion-terminated $\beta2(2\times4)$ and $c(4\times4)$ reconstructions. All are constrained laterally to GaAs substrates. The resulting $T=0$ surface stability diagrams show the most stable surface reconstruction and composition as a function of the cation chemical potentials. Slightly different diagrams result depending on whether or not the surface is assumed to be in equilibrium with the bulk. The stability diagram where equilibrium is assumed shows that In segregates to the surface on the anion-terminated $\beta2(2\times4)$ and $c(4\times4)$ surfaces, and that Ga segregates on the cation-terminated $\beta2(4\times2)$ surface. The (2×2) reconstructed surface shows little surface segregation. The larger surface unit cells make bulk-equivalent cation sites inequivalent at or near the surface. This leads to surface ordering that takes the form of layers with CuPt-like structure. We find strong $CuPt_B$ ordering in the surface layer of the (2×2) surface and the third subsurface layer of the $\beta2(2\times4)$ surface. Strong $CuPt_A$ ordering is found in the second subsurface layer of the $c(4\times4)$ surface. Weak ordering is also predicted in the second subsurface layer of the $\beta2(4\times2)$ surface.

ACKNOWLEDGMENTS

We acknowledge support by the U.S. DOE under Contract No. DE-AC36-83-CH10093. The authors are grateful to C. Wolverton and D. M. Wood for providing comments on the manuscript.

[1] T. Hashizume, Q. K. Xue, J. Zhou, A. Ichimiya, and T. Sakurai, Phys. Rev. Lett. **73**, 2208 (1994).
[2] Q. Xue, T. Hashizume, J. M. Zhou, T. Sakata, T. Ohno, and T. Sakurai, Phys. Rev. Lett. **74**, 3177 (1995), and references therein.
[3] J. M. Moison and M. Bensoussan, Surf. Sci. **168**, 68 (1986).
[4] X.-F. Jin, M.-R. Yu, F.-R. Zhu, and X. Wang, Semicond. Sci. Technol. **1**, 293 (1986).
[5] See, for instance, U. Bardi, Rep. Prog. Phys. **57**, 939 (1994).
[6] J. M. Moison, C. Guille, F. Houzay, F. Barthe, and M. Van Rompay, Phys. Rev. B **40**, 6149 (1989).
[7] J. M. Moison, F. Houzay, F. Barthe, J. M. Gerard, B. Jusserand, J. Massies, and F. S. Turco-Sandroff, J. Cryst. Growth **111**, 141 (1991).
[8] K. Muraki, S. Fukatsu, Y. Shiraki, and R. Ito, Appl. Phys. Lett. **61**, 557 (1992).
[9] J. Nagle, J. P. Landesman, M. Larive, C. Mottet, and P. Bois, J. Cryst. Growth **127**, 550 (1993).
[10] J.-M. Gerard, C. d'Anterroches, and J.-Y. Marzin, J. Cryst. Growth **127**, 536 (1993).
[11] See, for instance, A. Zunger, and S. Mahajan, in *Handbook on Semiconductors*, edited by T. S. Moss (Elsevier, Amsterdam, 1994), p. 1399, and references therein.
[12] S. Froyen and A. Zunger, Phys. Rev. Lett. **66**, 2132 (1991).
[13] J. E. Bernard, S. Froyen, and A. Zunger, Phys. Rev. B **44**, 11 178 (1991).
[14] R. Osório, J. E. Bernard, S. Froyen, and A. Zunger, Phys. Rev. B **45**, 11 173 (1992).
[15] S. Froyen, J. E. Bernard, R. Osório, and A. Zunger, Phys. Scr. **T45**, 272 (1992).
[16] M. D. Pashley, Phys. Rev. B **40**, 10 481 (1989).
[17] We convert the top four layers of the GaP $\beta2(2\times4)$ surface to the InP $\beta2(2\times4)$ surface by removing 12 Ga and adding 14 In and 6 P per unit cell.
[18] We used the orthorhombic forms of Ga and (black) P and the tetragonal form for In.
[19] M. Tmar, A. Gabriel, C. Chatillon, and I. Ansara, J. Cryst. Growth **69**, 421 (1984).
[20] M. Tmar, A. Gabriel, C. Chatillon, and I. Ansara, J. Cryst. Growth **68**, 557 (1984).
[21] J. E. Northrup and S. Froyen, Phys. Rev. Lett. **71**, 2276 (1993).
[22] J. E. Northrup and S. Froyen, Phys. Rev. B **50**, 2015 (1994).
[23] The allowed ranges are smaller than the bulk formation energies (by 60 and 30 meV for GaP and InP, respectively) because of the lateral constraint to GaAs.
[24] Z. W. Lu, D. B. Laks, S.-H. Wei, and A. Zunger, Phys. Rev. B **50**, 6642 (1994).
[25] S.-H. Wei (private communication).
[26] We have ignored the fact that the two sites on each dimer are inequivalent because, by examination, their geometries are very similar.
[27] The extra electron on the raised dimer on the (2×2) surface is taken up by the P dangling bonds on the $\beta2(4\times2)$ surface.
[28] The fact that the unconfined sp^2 site on the high dimer on the (2×2) surface transforms at a much larger value of $\Delta\mu$ than the confined sp^2 sites on low dimers on the (2×2) and the $\beta2(4\times2)$ surfaces shows that it must be the size difference and not the electronic difference between Ga and In that determine how the various dimer sites are occupied.
[29] A quantitative spin model, modeling the energies of sites A–D, was fit to the first-principles calculations. The model, which is similar to the one in Ref. 14, indicates that intersite interaction terms are smaller than 1 meV. The model was used to compute the energies of the surfaces that are shown as dashed lines in Fig. 5(a).
[30] Again, the fact that there are two types of threefold sites and two types of fourfold sites has been ignored because, by examination, their geometries are very similar.
[31] The bulk mixing enthalpy is proportional to $x(1-x)$, and the mixing entropy is just the ideal entropy $kT[\,x\ln x+(1-x)\ln(1-x)]$.
[32] L. G. Ferreira, S.-H. Wei, and A. Zunger, Phys. Rev. B **40**, 3197 (1989).
[33] E. Tournie, A. Trampert, and K. H. Ploog, Europhys. Lett. **25**, 663 (1994).